Accepted Manuscript

Extra tension at electrode-nanowire adhesive contacts in nano-electromechanical devices

Alexander I. Livshits, Liga Jasulaneca, Jelena Kosmaca, Raimonds Meija, Justin D. Holmes, Donats Erts

PII: S0997-7538(17)30057-8

DOI: 10.1016/j.euromechsol.2017.08.009

Reference: EJMSOL 3477

To appear in: *European Journal of Mechanics / A Solids*

Received Date: 23 January 2017

Revised Date: 10 August 2017

Accepted Date: 14 August 2017

Please cite this article as: Livshits, A.I., Jasulaneca, L., Kosmaca, J., Meija, R., Holmes, J.D., Erts, D., Extra tension at electrode-nanowire adhesive contacts in nano-electromechanical devices, *European Journal of Mechanics / A Solids* (2017), doi: 10.1016/j.euromechsol.2017.08.009.

Extra tension at electrode-nanowire adhesive contacts in nano-electromechanical devices

Alexander I. Livshits[a], Liga Jasulaneca[a], Jelena Kosmaca[a,*], Raimonds Meija[a], Justin D. Holmes[c,d], and Donats Erts[a,b]

[a] Institute of Chemical Physics, University of Latvia, Riga, 19 Raina Blvd., LV 1586, Latvia

[b] Department of Chemistry, University of Latvia, Riga, 1 Jelgavas Str., LV 1004, Latvia

[c] CRANN & AMBER, Trinity College Dublin, Dublin 2, Ireland

[d] Department of Chemistry and Tyndall National Institute, University College Cork, Cork, Ireland

*Corresponding author. E-mail: jelena.kosmaca@lu.lv; Tel.: +37167033936.

Abstract

We report a strong tangential component of the reaction force at electrode to nanowire adhesive contact which was previously established using electrostatic attraction. The reaction force tangential component absolute value was found to be comparable to or even bigger than the corresponding normal component. This effect is important for understanding of the mechanics of nano-electromechanical devices. Both the experiment and the corresponding theory are presented. Fitting of the obtained analytical solutions to experimental data was used to measure the reaction force acting at the contact for several nanowire-electrode configurations.

Keywords: nano-electromechanical contact; nano-electromechanical switch; nanowire deflection.

1. Introduction

Nano-electromechanical systems (NEMS) utilize electrical and mechanical properties of nanomaterials for nanoscale devices. Their operation involves electromechanically driven motion of an active element, such as a nanowire or a nanotube. Current examples of NEMS include a range of nanorelays and switches (ON-OFF devices) [1–12]. These devices are an alternative to the complementary metal-oxide-semiconductor (CMOS) devices, for example, for memory applications [1, 10, 13]. Despite the benefits of the NEMS technology, which include further miniaturisation, significant reduction of power consumption and ability to operate in harsh environmental conditions, their reliability is still a critical issue [1]. Failing due to adhesion, conductivity reduction due to surface wear and/or contamination, switching element burn-out due to electrical discharge and Joule heating are typical problems of NEMS. Solution of these problems requires a better understanding of the mechanics of NEMS and in particular of the conditions at the contacts.

Various systems, including carbon nanotubes, as well as metal and semiconductor nanowires, have been used as active components in NEM switches [1–6, 13–15]. In the majority of cases such active elements can be considered as straight objects (thin rods), cylindrical or rectangular in cross-section. In these cases, usual linear beam bending theory can be used to describe their mechanical behaviour. In many cases, however, mechanical behaviour of the active element in a pre-bent configuration is the subject of interest.

A gateless two-source controlled nano-electromechanical switch based on individual, single-clamped Ge nanowire [5, 7, 16] is an example of such a case. Initially the nanowire and the electrode are physically separated, representing an “off” state. Switching the device to an “on” state is achieved by applying an electrostatic potential between the single clamped active element (the source) and the electrode (the drain). If the applied voltage achieves a certain value, the jump-to-contact happens and after the voltage is switched off the device remains in the “on” state due to adhesion forces.

The scheme shown in Figure 1 is equally applicable to nanorelays and two input switches. However, the shape and placement of electrodes may be different. In Figure 1, the elastic beam, representing a nanowire, is fixed at a macroscopic electrode on the left. The beam is bent and kept in contact with another electrode on the right (Electrode 1 on Figure 1) by the adhesion force. In case of nanorelays an additional electrode (Electrode 2 on Figure 1) is needed to detach the active element from the contact.

The detachment is achieved by applying an electric voltage pulse between the active element and the additional electrode. The latter cannot be reached by the nanowire. For the contrary, in case of nanoswitch the nanowire is supposed to establish contact with each of the electrodes in turn.

One of the reported difficulties [16]in the implementation of this scheme is the high voltage between the Electrode 2 and the nanowire, required to pull the latter from the contact. A novelty idea demonstrated in [16] for substantial reduction of the pull-off voltage without compromising the quality of the contact is to make use of mechanical resonance. Such a resonance can be generated by combination of DC/AC electrical fields. The pull-off voltages reported in [16] are much lower compared to static-only NEMS switching devices. Though this result can be considered as a success, it also demonstrates that in other circumstances both unwanted mechanical and electrostatic interaction can compromise the stability of the contact. No attempts were made in [16] to investigate the proposed mechanism theoretically. There were two reasons for that. First, it is necessary to describe the oscillations of the bent, while in contact, nanowire with full account of its curvature. Second, the conditions at the contact should be specially investigated because the magnitude and direction of the reaction force acting on the nanowire are unknown.

The knowledge of the reaction force at the contact has much more general applicability for NEMS development than the example which has been just described. Any atomic scale consideration of the processes at the contact requires a realistic macroscopic environment model to be imbedded in. The stress field around the contact is an important characteristic of such environment.

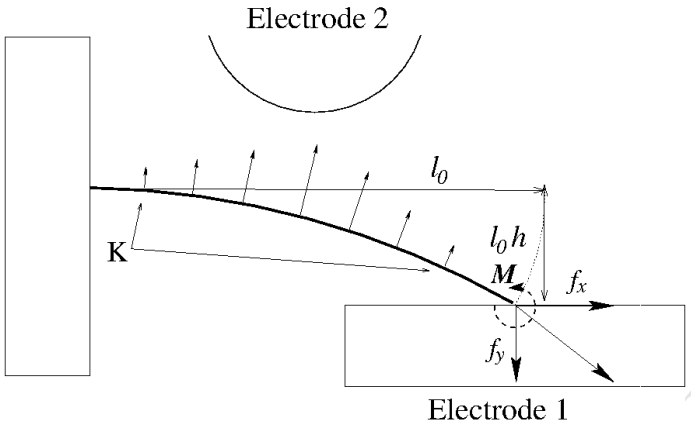

Fig. 1 Scheme of a gateless two input nanoswitch. l_0 – nanowire length, h – dimensionless vertical deflection, K – density of a distributed external force, usually of electrostatic nature, f_x and f_y - components of the reaction force at the contact, $\boldsymbol{M}$ – force moment at the contact

In this work, we first report an experiment. It shows that the reaction force, which an active element experiences at the contact, may contribute not only to its bending, but also to its axial tension. Second, a nonlinear equation of motion for the active element of a nanoswitch is derived. It takes full account of the curvature of the element and is exact in this sense. It also incorporates the roles of the pull-off force, of the reaction force and of the possible force moment at the contact. Third, a static solution of the problem is obtained and compared to the experimental shape of the nano element. The result of such a comparison allows us to estimate both normal and tangential components of the reaction force as well as the bending moment acting on the nanowire at the contact. Forth, small oscillations of the nanowire which is brought to contact with the electrode are considered. This leads us to an analytical formula for the nanowire resonant oscillation frequency as a function of deflection, reaction force and the force moment acting at the contact.

2. Methods

2.1. Experimental

Monocrystalline Ge nanowires were grown using the supercritical fluid method [17]. The nanowires were suspended on a TEM grid surface pre-coated with a 5/20 nm thick Pt/Au layer (Gatan 682 PECS) and investigated in a scanning electron microscope (Hitachi S-4800 SEM) in order to select a suitable

nanowire. The end of the selected nanowire was clamped at the edge of the grid with a platinum strip applying the focused ion beam technique (SEM-FIB TECNAI LYRA). The width of the strip exceeded the nanowire diameter which is sufficient to make the end of the nanowire fixed [18, 19].

The switch elements were attached to positioners of a SmarAct 13D nanomanipulation system and staged inside the Hitachi S-4800 SEM equipped with Fisher electrical connectors in the walls of the specimen chamber, to control the stage and apply the voltage. Fine positioner's adjustment in range from several mm to a few nm allowed us to configure the measurement setup *in-situ* [16, 19-22]. A Pt/Au coated silicon chip was used as a plane counter electrode (Electrode 1 in figure 1). It was connected to Keithley-6430 DC voltage source. An electrochemically etched Au tip was grounded and used to ensure that the nanowire deflection occurs in plane. Continuous visualisation and imaging in SEM was used to control the setup configuration, determine nanowire size and shape during the experimental session. In particular, the length of the chosen nanowire was estimated as l_0*=138.7±0.1 µm* and the radius as *r=99±2 nm*. At the beginning of the experiment single clamped nanowire's resonant frequency was obtained by exciting the nanowire oscillations electrostatically. The nanowire's resonance was detected as a sharp increase of the nanowire oscillation amplitude at a certain AC frequency. This frequency was found to be equal to *7.31±0.01 kHz*. This would give the estimation of the Young's modulus *E=137±7 GPa* assuming that the nanowire's mass density is equal to the bulk value of Ge *ρ=5323 kg/*m^{3}and no surface layer, with mechanical properties different from the bulk, exists. In fact, some oxide layer was definitely present. All of the preparations and measurements mentioned above have been done for five similar nanowires. It has been found that for a single clamped nanowire two slightly different (not more than by 10%) resonant frequencies can be detected. They correspond to oscillations in perpendicular planes. This is a consequence of the imperfection of the nanowire's cylindrical symmetry. For the finally chosen sample we were unable to detect any difference between these frequencies.

Further measurements were performed in the following steps. 1) The plane electrode and the Au tip were moved towards the nanowire. 2) A DC voltage sweep starting from 0 V with a step width 0.1 V was applied between the plane electrode and the nanowire until the nanowire right end jumped into contact with the electrode surface. 3) The nanowire deflection was determined by comparing the SEM images before and after establishing the contact (Fig. 2). The deflection was measured in thirteen to fifteen

points evenly distributed along the whole nanowire length. On Figure 2, *H* represents the deflection at the point of the nanowire right end. 5) The AC voltage of 2 V was applied between the Au tip and the rest of the system and the resonance frequency of the nanowire was determined. 6) The AC voltage of 1 V was applied between the Au tip and the rest of the system and the resonance frequency of the nanowire was determined once more. 7) The plane electrode was moved away from the nanowire until detachment happened.

These steps were repeated for a set of right end dimensionless deflection *h* (ratio of the deflection over the nanowire length l_0) absolute values increasing from 0.05 to 0.35. Then the procedure was repeated for a set of decreasing absolute values of *h* chosen in the same interval.

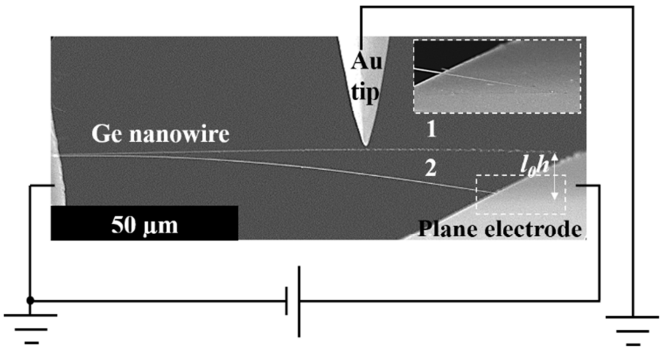

Fig.2 Schematic of the experimental setup with over layered SEM images. The nanowire before (position 1) and after (position 2) establishing the contact with the plane electrode. The left end of the nanowire is fixed, whilst the right end, when the voltage is applied, consequently bends and jumps into contact with the plane electrode. The inset shows the nanowire's right end in contact with the electrode. Comparison of the nanowire shape in positions 1 and 2 is used for determination of the nanowire deflection along the whole nanowire length.l_0h represents the deflection at the point of the nanowire right end

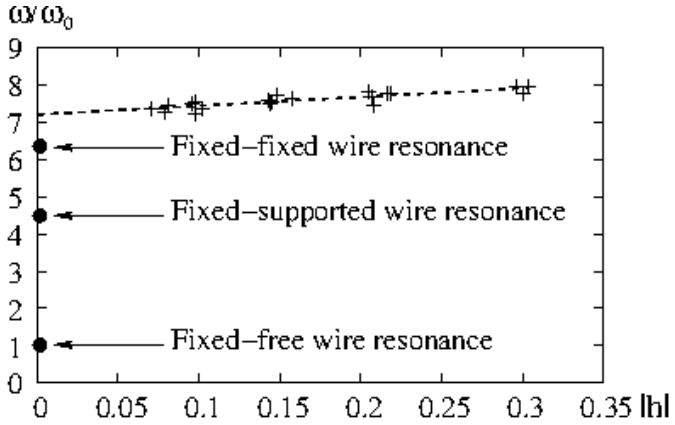

Fig. 3 Ratio of the resonant frequency – ω to that of the single-clamped nanowire – ω_0 as a function of deflection *h*. Black circles correspond to the "fixed-free", "fixed-supported" and "fixed-fixed" resonances of a straight thin rod without any axial stress. The dashed line represents the best fit of a linear function to the experimental data.

On Figure 3 it is clearly seen that the measured resonance frequencies of the Ge nanowire are higher than the frequency of the "fixed-fixed" configuration and they are further growing with the value of the deflection *h*. In [19] slightly different experiment has been reported. A similar Ge nanowire was brought to contact with a counter electrode purely mechanically. The electrode was moved towards the nanowire until the contact has been established by adhesion forces. The electrostatic attraction was not employed in that experiment. The authors measured the resonance frequency and then applied some electric voltage pulse, which resulted in current flowing through the contact area. They repeated these measurements several times with increasing voltages applied. The main observation of that experiment was that the resonant frequency of the nanowire was growing each time after the voltage has been increased. The initial frequency was close to that of a "fixed-supported" rod and it approached the "fixed-fixed" value after several cycles. The conclusion of the authors was that the strength of the adhesion was increased as a result of electric current flow through the contact area.

In our experiment the nanowire has been brought to contact by electrostatic forces. Though the voltage was switched off after each jump-to-contact event, the electric current had enough time to modify the contact properties and some adhesion strengthening could be expected. It however cannot result in resonant frequencies being higher than that of the "fixed-fixed" configuration, unless the nanowire is experiencing an axial stretching or its linear density and/or Young's modulus are not constant. This subject is further discussed in our last section, after the corresponding theory is presented.

2.2. Theoretical basis

2.2.1. The equation of motion. The subject of our attention is the shape of a nanowire, while the latter is kept in contact with the electrode by adhesion forces. The nanowire may have a surface layer (oxide shell) with mechanical properties which differ from those of the core. This is why mass density ρ in all of the expressions below must be interpreted as an effective value. Flexural rigidity R for homogeneous rods is given by formula (1a). For the case of circular cross-section wire with core-shell model it is given by formula (1b) [23]. For the limiting case of very thin shell, (1b) reduces to a simple expression (1c) [24].

$$R = EI, \quad I = \frac{\pi D^4}{64} \tag{1a}$$

$$R = \frac{1}{64}\pi E^c D^4 + \pi E^s s\left(\frac{1}{8}D^3 + \frac{3}{8}D^2 s + \frac{1}{2}Ds^2 + \frac{1}{4}s^3\right), \tag{1b}$$

$$R = \frac{1}{64}\pi E^c D^4\left(1 + \frac{8sE^s}{E^c D}\right). \tag{1c}$$

E^c, E^s - stands for the Young's modulus of the core and shell correspondingly, D - is the core diameter, s – is the shell thickness. It must be said that the formula (1b) cannot be interpreted as (1a) with some kind of effective Young's modulus. This is because the effective value, which would be introduced this way, contradicts with the Young's modulus definition. If used, it would result in a wrong elongation of the rod under tension. To make our expressions general the flexural rigidity R will be used everywhere.

Beam bending [25] is described in the spirit of the well-known Euler-Bernoulli theory, however, in its nonlinear generalized form. A short derivation of the main equation is presented below. We start with the equilibrium equation for a cylindrical beam and the expression for the bending moment [26]:

$$R\left[\frac{dr}{dl}\times\frac{d^3r}{dl^3}\right]=\left[\tilde{F}\times\frac{dr}{dl}\right]$$
$$\frac{d\tilde{F}}{dl}=-\tilde{K} \qquad (2a)$$

$$\tilde{M}=R\left[\frac{dr}{dl}\times\frac{d^2r}{dl^2}\right] \qquad (2b)$$

The vector *r* is representing the coordinates of a point on a beam which is considered as a 1-D object, $\tilde{K}$– is a linear density of the external force $\tilde{F}$,*l*– is a coordinate along the beam. We assume that at the left end the beam is always parallel to *x* axis and that all of the deformation takes place in *xy* plane, so that the *r* has no *z* component.

Taking a derivative of the equation (2a), equation (3) can be written. The *X* and *Y* are the corresponding components of ***r.*** Starting from here all length related variables are expressed in units of the nanowire length $\xi=l/l_0$

$$X^{(1)}Y^{(4)}-X^{(4)}Y^{(1)}+X^{(2)}Y^{(3)}-X^{(3)}Y^{(2)}-$$
$$F_xY^{(2)}-F_yX^{(2)}+K_xY^{(1)}-K_yX^{(1)}=0 \qquad (3)$$
$$\begin{pmatrix}F_x\\F_y\end{pmatrix}=\frac{l_0^2}{R}\begin{pmatrix}\tilde{F}_x\\\tilde{F}_y\end{pmatrix},\quad\begin{pmatrix}K_x\\K_y\end{pmatrix}=\frac{l_0^3}{R}\begin{pmatrix}\tilde{K}_x\\\tilde{K}_y\end{pmatrix}$$

All derivatives are presented as upper indices in brackets and are taken with respect to the normalized coordinate ξ – along the beam.

Using an evident equality (4) all the derivatives of *X* can be expressed in terms of the derivatives of *Y*.

$$\left(X^{(1)}\right)^2+\left(Y^{(1)}\right)^2=1 \qquad (4)$$

This leads to (5).

$$\left(\frac{Y^{(2)}}{X^{(1)}}\right)^{(2)} - \frac{F_{tens}}{X^{(1)}}Y^{(2)} + K_x Y^{(1)} - K_y X^{(1)} = 0$$

$$F_{tens} = F_x X^{(1)} + F_y Y^{(1)};\ X^{(1)} = \sqrt{1-\left(Y^{(1)}\right)^2};\qquad X(l) = \int_0^l X^{(1)} dx \tag{5}$$

Equation (5) in the case of small deflections can be written in a well recognizable linear form of (6).

$$Y^{(4)} - F_x Y^{(2)} - K_y = 0 \tag{6}$$

Expressions for the transverse force are given in (7). The force acting on the beam has both concentrated and distributed components. The former is due to adhesion and short range repulsion. This force acts at the contact point and may contribute both to bending and axial tension. Two constants – *(f_x, f_y)* are used in (7) and below to characterize this force.

The distributed force density *K*, if present, may have contributions of different nature. An externally applied force, usually of electrostatic nature, is one of such contributions. It is strictly perpendicular to the nanowire axis and directed towards the Electrode 2. For a given shape of the beam this force density is described by a scalar function $g(\xi,t)$. If the nanowire is in motion the inertial and dissipative contributions to the force density should also be taken into account. In (7) they are represented by the corresponding time derivatives of the coordinates.

$$F_x = f_x + \int_\xi^1 K_x(u)du,\quad F_y = f_y + \int_\xi^1 K_y(u)du$$

$$K_x = -\mu Y^{(1)} - \ddot{X} - 2\lambda\dot{X}$$

$$K_y = \mu X^{(1)} - \ddot{Y} - 2\lambda\dot{Y}$$

$$\dot{X}(\xi,t) = -\int_0^\xi \frac{Y^{(1)}\dot{Y}^{(1)}}{X^{(1)}}du \tag{7}$$

$$\ddot{X}(\xi,t) = -\int_0^\xi \frac{Y^{(1)}\ddot{Y}^{(1)}}{X^{(1)}} + \frac{\left(\dot{Y}^{(1)}\right)^2}{\left(X^{(1)}\right)^3}du$$

$$T = l_0^2\sqrt{\frac{m}{R}},\quad \mu = \frac{l_0^3 g(\xi,t)}{R},\quad \lambda = \frac{l_0 c}{2\sqrt{Rm}}$$

In (7) the nanowire linear mass density - $m=\pi D^2\rho/4$, the dissipative coefficient - *c* and the time unit – *T* have been introduced. The time derivatives are represented as dots over the corresponding function. Substitution of the first two expressions of (7) into the equilibrium equation (2a) leads to (8).

$$X^{(1)}Y^{(3)} - Y^{(1)}X^{(3)} = f_x Y^{(1)} - f_y X^{(1)} + Y^{(1)}\int_{\xi}^{1} K_x(u)du - X^{(1)}\int_{\xi}^{1} K_y(u)du \tag{8}$$

At $\xi = 1$ the equation (8) can be reduced to (9).

$$f_y = -\left(\left[\frac{Y^{(3)}}{X^{(1)2}} + \frac{Y^{(1)}Y^{(2)^2}}{X^{(1)4}}\right] + f_x \frac{Y^{(1)}}{X^{(1)}}\right)_{\xi=1} \tag{9}$$

If the right end of the nanowire is free, the equation (9) reduces to usual “free end” boundary conditions (10).

$$Y^{(2)}(1) = Y^{(3)}(1) = 0 \tag{10}$$

If, however, it is in contact, the equation (9) allows us to eliminate the unknown f_y force component from the equation. Using (9) and (7) the equation of motion can be finally written in terms of *y*-displacement, its time and coordinate derivatives and integrals.

$$\begin{gathered}\left(\ddot{Y} + 2\lambda\dot{Y}\right)X^{(1)} + Y^{(1)}\int_{0}^{\xi}\frac{Y^{(1)}\left(\ddot{Y} + 2\lambda\dot{Y}\right)}{X^{(1)}} + \frac{\left(\dot{Y}^{(1)}\right)^2}{\left(X^{(1)}\right)^3}du + \\ \left(\frac{Y^{(2)}}{X^{(1)}}\right)^{(2)} - F_{tens}\frac{Y^{(2)}}{X^{(1)}} = \mu \\ F_{tens} = X^{(1)}\int_{\xi}^{1} K_x du + Y^{(1)}\int_{\xi}^{1} K_y du + \frac{f_x\left(X^{(1)}(1)X^{(1)} + Y^{(1)}(1)Y^{(1)}\right)}{X^{(1)}(1)} - \\ \left[\frac{Y^{(3)}}{X^{(1)2}} + \frac{Y^{(1)}Y^{(2)2}}{X^{(1)4}}\right]_{\xi=1} Y^{(1)}\end{gathered} \tag{11}$$

Unlike in the recent work [27], the equation (11) is exact with respect to curvature. It does not contain any truncated expansions. This is achieved because of the use of the proper coordinate $\xi = l / l_0$ instead of the Cartesian *x*. Equation (11) does not describe the effect of axial elongation due to tension. This usually negligible effect can be accounted for when the solution of the problem has been obtained. Similar to (5) and (6), for small deflections equation (11) can be written in a well recognizable linear form:

$$\ddot{Y} + 2\lambda\dot{Y} + Y^{(4)} - f_x Y^{(2)} = \mu$$

2.2.2. Static solution. If the external field is constant in time and a static solution only is to be found, the equation (11) reduces to (12).

$$\left(\frac{Y^{(2)}}{X^{(1)}}\right)^{(2)} - F_{tens}\frac{Y^{(2)}}{X^{(1)}} = \mu(\xi)$$

$$F_{tens} = -X^{(1)}\int_{\xi}^{1}\mu Y^{(1)}du + Y^{(1)}\int_{\xi}^{1}\mu X^{(1)}du - \left[\frac{Y^{(3)}}{X^{(1)2}} + \frac{Y^{(1)}Y^{(2)2}}{X^{(1)4}}\right]_{\xi=1} Y^{(1)} + \frac{f_x\left(X^{(1)}(1)X^{(1)} + Y^{(1)}(1)Y^{(1)}\right)}{X^{(1)}(1)} \quad (12)$$

The distributed external force μ is usually of electrostatic nature. For a particular configuration, it should be obtained numerically as a solution of the corresponding 3-D electrostatic problem. A simple model of such a force is used in this work for general analysis. The force density is represented as an intensity multiplier times some normalized function. This function should be positive, have one extremum and approach zero on both ends of the nanowire. This is because the electrostatic force is directed normal to the surface and this normal changes direction at both ends of the nanowire. To make things simple this function is modelled by a polynomial expression and by Dirac Delta function (13).

$$\mu_n(\xi) = \mu_0\frac{(n!)^2}{(2n+1)!}(\xi(1-\xi))^n, \quad n = 1, 2,...$$
$$\mu_\infty(\xi) = \mu_0\delta\left(\xi - 1/2\right) \quad (13)$$

At the left end the boundary conditions are trivial.

$$Y(0) = 0; \quad \left(Y^{(1)}\right)_{\xi=0} = 0 \quad (14)$$

The boundary conditions on the right end depend on the physical model under consideration. In this work, it is assumed that the *y* coordinate of the beam at contact is known.

If the switch contact takes place at the very end of the beam and the length of the contact along the beam is short enough, then the tangential vector of the beam does not need to be parallel to the electrode surface and so, unlike in (14), the first derivative is unknown. In this case the bending moment at contact point should be used instead. Using expressions (2b) and (4) the boundary conditions can be written as (15), where *h* is the distance (dimensionless value) between the *x* axis and the surface of the electrode.

$$Y(1)=h$$

$$\left(\frac{Y^{(2)}}{X^{(1)}}\right)_{\xi=1}=\frac{l_0\tilde{M}_z}{R}=M \tag{15}$$

The second expression in (15) becomes linear only if the bending moment is neglected. This however is usually not possible for nano-electromechanical devices due to physical reasons. The repulsive component of the reaction force, because of its short range, can be treated as one applied at a well-defined position – at the point of contact. The attractive component however has longer range. Its "centre of mass" may be close to the point of contact, but does not coincide with it. Thus, in general the pair of forces leads to appearance of some bending moment.

Equation (12), together with the boundary conditions (14) and (15), determine the shape of the bent nanowire brought to contact with an electrode. This shape is dependent on four parameters: f_x– the tangential component of the reaction force at contact, M – the bending moment, h– the deflection and μ_0 – the intensity of the external distributed force.

Solution of the problem can be obtained as an expansion (16).

$$Y(\xi)=\sum_{i,j,k=0,i+j+k>0}^{i,j,k=\infty}\mu_0^i h^j M^k y_{ijk}(\xi) \tag{16}$$

It appeared however that the complexity of the solution so rapidly grows with indices that it becomes impossible to use more than the three leading terms. Even these terms are complicated enough to make direct calculations problematic due to numerical loss of precision. At the same time, it is easy to show that in the case of $f_x=0$ the solution reduces to a set of polynomials.

Taking into account the fact that the tangential component of the reaction force at contact is supposed to be small and in any case, is limited by the static friction, it is also treated as an expansion parameter. In this way, all of the solution components become polynomials, which can be obtained with the help of any computer algebra system.

$$Y(\xi)=\sum_{i,j,k,l=0,i+j+k+l>0}^{i,j,k,l=\infty}\mu_0^i h^j M^k f_x^l y_{ijkl}(\xi) \tag{17}$$

Several analytically obtained members of the expansion (17) can be found in the Appendix.

As it can be seen in Figure 4, the expansion in *h* up to the order of five has been practically converged even for the unrealistically big deflection of *h=0.65*. The graphs which are shown in Figure 4 correspond to the situation when neither forces parallel to the electrode surface nor distributed electrostatic force are applied. Figure 5 demonstrates the effect of a force parallel to the electrode surface. The same deflection value of *h=0.65* have been chosen. The solutions shown are of the fifth order in deflection and they correspond to three values of the force f_x*= [3, 0, -3]*.

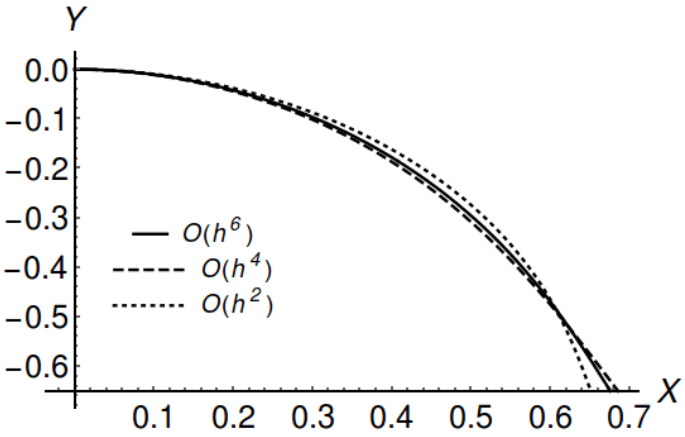

Fig.4 Static deflection solutions up to the first –"O(h^2)", third –"O(h^4)"and fifth –"O(h^6)" order in deflection *h. h=0.65,* f_x*=0*

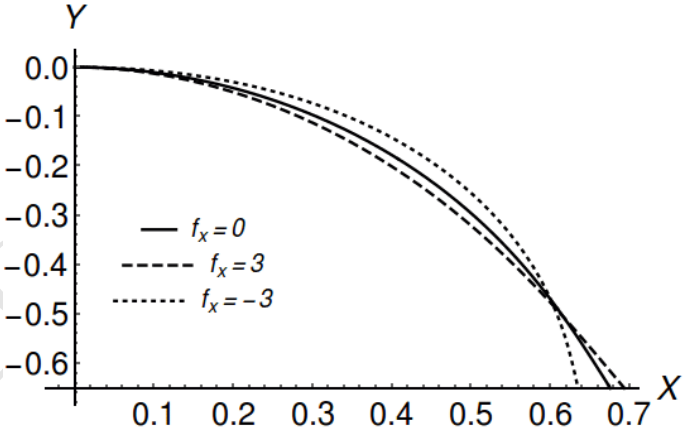

Fig.5 The influence of the static friction force on the nanowire shape. The example solutions are of the fifth order of both deflection and force. Deflection *h=0.65*

In Figure 6 the effect of the bending moment *M* and the tangential force are shown. It is important that when the bending moment is applied, the contact point on the electrode changes position. To keep

in our simulations, the contact position the same it is necessary to use some tangential reaction force as well.

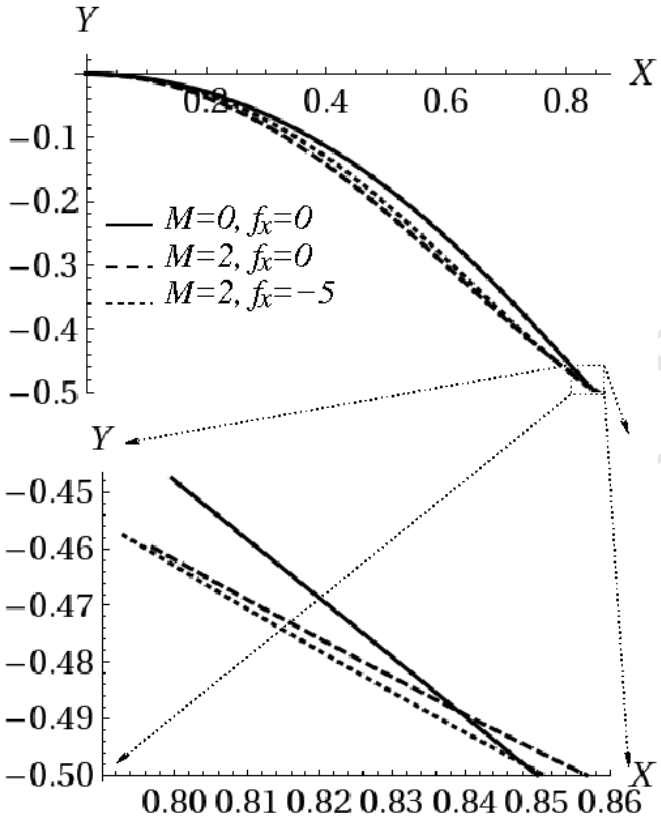

Fig.6 The influence of bending moment and of tangential reaction force on the nanowire shape. Example solutions of the third order of deflection are shown. Deflection *h=-0.5*. Solid line: *M=0, f_x=0*. Dashed line: *M=2, f_x=0*. Dotted line: *M=2, f_x=-5*. Inset – contact point vicinity

Substitution of solution into the expressions (12) results in tension force formula. The result is rather lengthy and is not presented here but can be easily reproduced. An important consequence of it is that unlike in the case of a musical instrument string, the tension is not constant along the nanowire length. The averaged along the whole length tension force is given by expressions (18) where only linear and quadratic terms are shown for several model external distributed force functions.

$$\left\langle F_{tens}\right\rangle = f_x + 3h^2 - \frac{3}{2}hM + \begin{cases} -\frac{3}{5}h\mu_0 - M\frac{\mu_0}{40} + \frac{2}{315}\mu_0^2 & n=1 \\ -\frac{33}{56}h\mu_0 - M\frac{\mu_0}{56} + \frac{1795}{288288}\mu_0^2 & \text{if} \quad n=2 \\ -\frac{51}{88}h\mu_0 - M\frac{\mu_0}{88} + \frac{26621}{4434144}\mu_0^2 & n=4 \end{cases} \qquad (18)$$

The formulas (18) demonstrate that the resonance frequency of a nanowire oscillations, while in contact, must depend on the deflection *h*, the bending moment *M*, the external force intensity μ_0 and the tangential reaction f_x.

2.2.3. Small oscillations. In this section the equilibrium static solution *S* is supposed to be known. The aim now is to obtain small oscillations around it induced by a harmonic in time external distributed force.

$$\mu(\xi,t) = \mu_{static}(\xi) + \mu_{dynamic}(\xi)\exp(-i\omega t) = (\mu_0 + \nu_0 \exp(-i\omega t))\frac{\mu(\xi)}{\langle\mu(\xi)\rangle} \quad (19)$$

The consequence of the electrostatic nature of the force is that the spatial distribution of the dynamic force is proportional to that of the static part. The intensity factors however must be taken as independent parameters because they depend on the choice of the AC and DC voltages applied.

The first dynamic correction to the static solution has been obtained in a form of truncated expansion in orders of amplitude of the time dependent part of the force.

$$Y(\xi,t) = S(\xi) + \nu_0 D(\xi,t) \quad (20)$$

$$\begin{aligned} &D(\xi,t) = \psi(\xi)\cos(\omega t) \\ &\psi(\xi) = N(\sin(\chi\xi) - \sinh(\chi\xi)) - \cos(\chi\xi) + \cosh(\chi\xi) \\ &N = \frac{\cos(\chi) - \cosh(\chi)}{\sin(\chi) - \sinh(\chi)} \end{aligned} \quad (21)$$

The result of the transformations mentioned above has a familiar general form of (22). It determines the value of the resonant frequency as a function of all of the parameters. Because the static solution is represented as a power expansion in its parameters, all of the coefficients in (22), for a given value of χ, have this structure.

$$A(\mu_0, h, M, f_x, \chi) + iB(\mu_0, h, M, f_x, \chi)\lambda\omega + C(\mu_0, h, M, f_x, \chi)\omega^2 = 0 \quad (22)$$

It must be said that in present work the dissipative coefficient λ is supposed to be negligible. That is because our estimation of the quality factor of our resonator is equal to at least several hundreds. So, the corresponding term in (22) is ignored.

The boundary conditions for the dynamic correction at $\xi = 0$ are trivial.

$$D(0,t) = D^{(1)}(\xi,t)\big|_{\xi=0} = 0 \quad (23)$$

At $\xi = 1$ however, two limiting cases are considered in this work. First, the conditions (24) will be considered. These conditions mean that both the bending moment and the deflection in this point are static. This case is denoted below as Case-1.

$$D(1,\mathrm{t}) = D^{(2)}(\xi,t)\Big|_{\xi=1} = 0 \tag{24}$$

For this case the parameter *k* is the smallest positive solution of the equation (25).

$$\begin{gathered}\cos(\chi)\sinh(\chi) - \sin(\chi)\cosh(\chi) = 0 \\ \chi \approx 3.92660231\ 2047918778\end{gathered} \tag{25}$$

Another right end boundary condition, considered here, means that the tangential direction of the nanowire is fixed at the static solution. The assumption behind this is that the nanowire is strongly bound to the electrode at the contact. This case is denoted below as Case-2.

$$D(1,t) = D^{(1)}(\xi,t)\big|_{\xi=1} = 0 \tag{26}$$

For this case χ must satisfy (27).

$$\begin{gathered}\cos(\chi)\cosh(\chi) = 1 \\ \chi \approx 4.73004074\ 4862704026\end{gathered} \tag{27}$$

In both cases the resonant frequency squared is obtained as a ratio of polynomials.

$$\omega^2 = \frac{\sum_{i,j,k,l} \alpha_{i,j,k,l} {\mu_0}^i {h^j} {M^k} {f_x}^l}{\sum_{i,j,k,l} \beta_{i,j,k,l} {\mu_0}^i {h^j} {M^k} {f_x}^l} \tag{28}$$

The most important terms of both the numerator and the denominator expansions for the resonant frequency square are given in the following tables. Universal coefficients – the ones that do not depend on the choice of the $\mu(\xi)$ function, are collected in Table 1. The coefficients which are $\mu(\xi)$- dependent are presented for two limiting cases. For the cases of constant force density and concentrated force applied at a half-length they are given in Table 2 and Table 3 correspondingly.

Table 1 Resonant frequency square expansion in h, M and f_x.

ijkl	Case-1, α	Case-1, β	Case-2, α	Case-2, β
0000	237.7210675	1	500.5639017	1
0001	11.51253004	0	12.30261862	0
0002	0	0	0	0
0010	0	0	0	0
0011	0	0	0	0
0020	272.2614859	-0.7220805270	584.8793026	-0.6218821707
0021	15.63575828	0.00428699475	0.09829446954	-0.001699025252
0100	0	0	0	0
0101	0	0	0	0
0110	-23.35824244	0.01569550281	47.92548197	0.04296501810
0111	1.216236798	0.00058214088	-4.402219269	-0.00106893613
0200	-6.528136623	-0.00203628349	2.709083522	-0.00195673476
0201	0.1741478139	0.000211419635	-0.2551818022	0.000202381769

Table 2 Resonant frequency square expansion members that are pull-off force dependent. Constant force-density case.

ijkl	Case-1, α	Case-1, β	Case-2, α	Case-2, β
1000	0	0	0	0
1001	0	0	0	0
1002	0	0	0	0
1010	-0.04018499464	0.0005325893955	-0.6676393260	0.0005029334646
1011	0.00841821066	-0.0000593130197	0.0000557155536	-0.008418210660
1100	-10.46078518	0.002083298739	-15.83077561	-0.002519552147
1101	-0.00695807957	-0.0001763587784	0.6272096067	0.0000671334406
2000	0.05709435166	-0.000044226255	0.0484289140	-0.0000401832005
2001	-0.00374210558	$4.484255673 \cdot 10^{-6}$	-0.004934568696	$4.123844225 \cdot 10^{-6}$

Table 3 Resonant frequency square expansion members that are pull-off force dependent. Concentrated force applied at the $\xi = {}^{1}/_{2}$ point.

ijkl	Case-1, α	Case-1, β	Case-2, α	Case-2, β
1000	0	0	0	0
1001	0	0	0	0
1002	0	0	0	0
1010	0.19644	0.000894776	-1.05732	0.000869091
1011	0.00156322	-0.00010094	0.113737	-0.0000960341
1100	-15.4466	0.00508259	-23.2536	-0.00309118
1101	-0.0356086	-0.000338252	1.05603	0.0000720121
2000	0.0966375	-0.000143836	0.132992	-0.000135408
2001	-0.00760279	0.0000135444	-0.0134202	0.0000127182

3. Results

The interpretation of the collected experimental data for the static nanowire shapes required two stages. Because all of the solutions obtained represent the nanowire shape in parametric form, the parameter values (the length along the nanowire from its left end to the data point) for all data points must be obtained first of all. For this to be done the experimental nanowire shape was approximated by a polynomial of the seventh order *P(x)*. According to boundary conditions (14) such a polynomial's youngest member is quadratic. The remaining six coefficients were routinely found using *Mathematica* [28] built in fitting procedure. Then, for each data point "*i*" the corresponding arc lengths has been obtained by integration.

$$\xi_i = \int_0^{x_i} \sqrt{1 + \left(\frac{dP(x)}{dx} \right)^2}\, dx \tag{29}$$

The solutions in the form of expansion (17) (first three members – of the first, third and fifth power in *h*and *M* and up to the fifths power in f_x) were used to approximate the obtained data sets (ξ_i, X_i, Y_i) with f_x and *M* as fitting parameters.

It was found that the experimental shape of the nanowire in contact can be reproduced by our analytical formulas only if some static friction force and some bending moment are applied at the contact. A typical example of the nanowire shape for deflection *h=0.21* is shown in Figure 7.

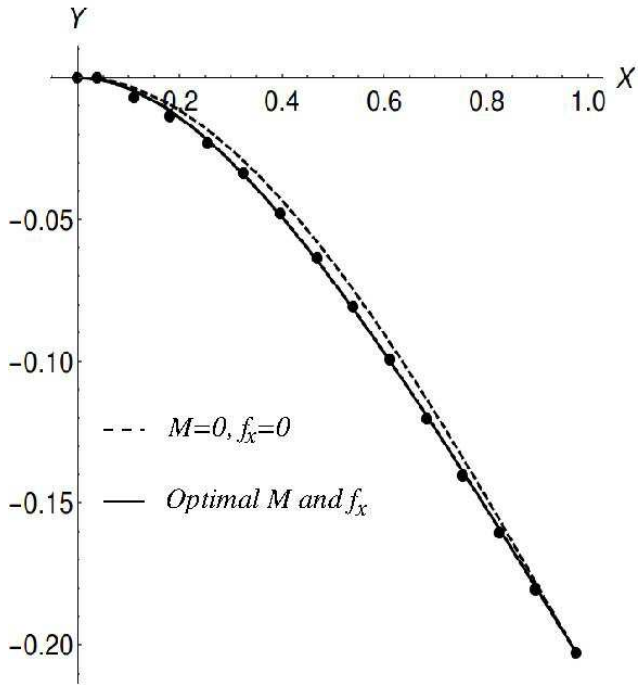

Fig. 7 Typical example of the nanowire shape while in contact. Circles - experimental points, dashed line – solution for $f_x = 0$ and $M=0$, solid line – fitted solution with the optimal f_x and ***M*** values for deflection $h=0.21$

The reaction force components as functions of deflection h, measured by curve fitting, are shown in Figure 8 and Figure 9.

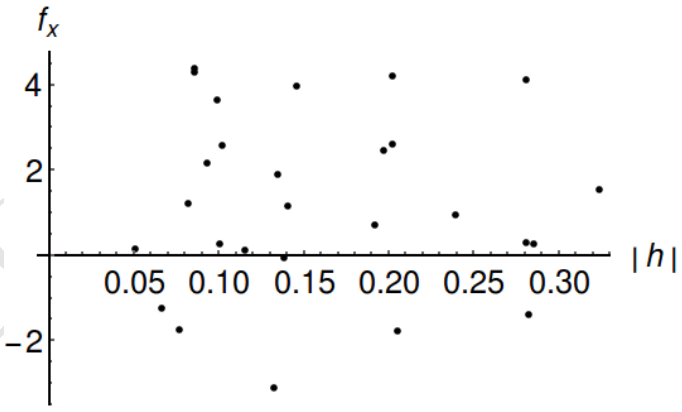

Fig. 8 Reaction force ***x*** component for a set of deflections (h)

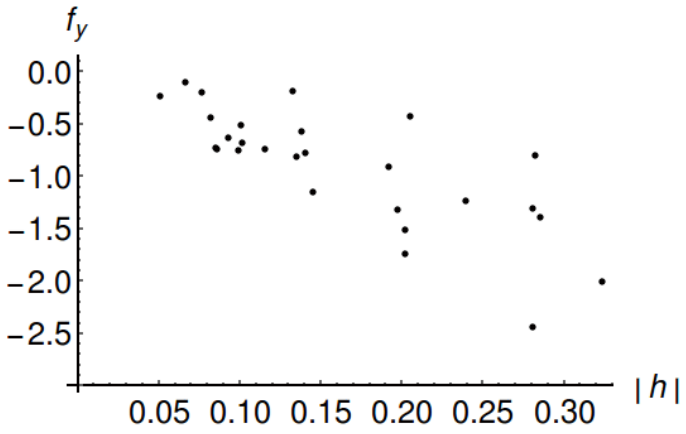

Fig. 9 Reaction force ***y*** component for a set of deflections (*h*)

The parallel to the electrode surface force component, i.e. static friction (Fig. 8), seems to be random. The value of this component may be positive or negative. It was a surprise for the authors to find that the absolute value of this force may be comparable or even bigger than that for the normal component. It is easy to see from the expression (9), that the normal reaction component which is required to keep the nanowire in contact with the electrode, is linearly dependent on the static friction. The bigger (positive) the f_x, the bigger (negative) the required f_y. On the other hand, because the f_x component may be negative, the corresponding f_y may be close to zero, or even positive. That means that in such a case the bent nanowire experiences axial contraction and applies pressure to the electrode.

The reaction force moment fitted values are shown in Figure 10. They are always positive. This is in agreement with the fact that the attractive forces are of long range compared to the repulsive ones and because of that their “centre of mass” is not at the very end of the nanowire.

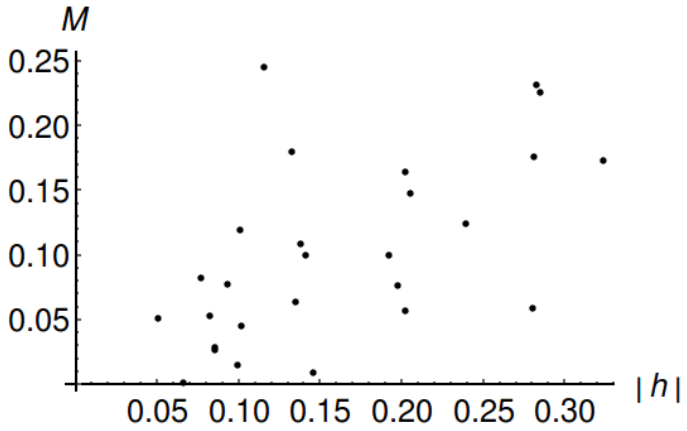

Fig.10 Reaction moment at the contact

As it was mentioned in the experiment section above, the nanowire deflection measurements were done by comparing the corresponding overlaid images. The accuracy of such measurement is limited. This can influence the accuracy of the optimal values of the parameters f_x and M obtained by fitting procedure. It is generally important to have an independent from the measurement confirmation of the reliability of results. The values of the fitted parameters, the expression (29) and the coefficients from Table 1 have been used to obtain the resonant frequencies of the nanowire for the whole set of deflections. The results are shown in Figure 11.

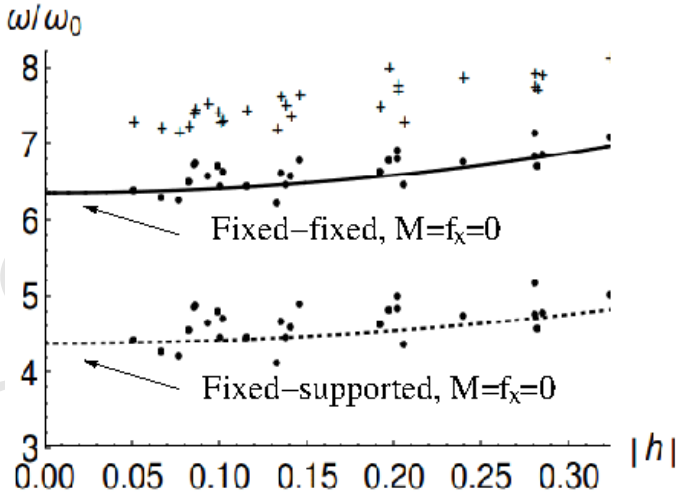

Fig. 11 The resonant frequencies. Experimental – the upper group, predicted with fixed-fixed boundary condition – the middle group, predicted with fixed-supported boundary condition – the lower group. The solid line – prediction for fixed-fixed boundary condition in while the dotted line – prediction for fixed-supported boundary condition the case of f_x=M=0

The upper group of points in Figure 11 represent our experimental results. The middle group is our prediction for the case of fixed-fixed boundary condition based on the obtained values of the reaction force f_x and moment M. Prediction for this boundary condition with $f_x = M = 0$ is shown as a solid line. The lower group of points and a dotted line represent the case of fixed-supported boundary condition. It is easy to see that our predicted values are representing the general tendency of frequency growth with deflection. The distribution of values due to variation of reaction force is also reproduced well. It however still should be explained why the experimental frequencies are about *15%* higher than the predicted ones.

4. Discussion

Better understanding of the mechanics and in particular contact mechanics of nano-system elements is vitally important for the NEMS development. Description of contact formation and termination is one of the challenging problems in this area. This problem can be approached on different levels and scales. A macroscopic approach of geometrically nonlinear beam bending theory has been used in this work. This is justified for long (with length to diameter ratio of more than a hundred) nanowires. One must be careful however in choosing the right elastic parameters for the material. This is because, at the nanoscale, surface effects become important and the bulk values may be inaccurate [29]. Current formulation is expected to yield accurate results for nanowires having diameters in range of tens nanometers, where these effects have only minor impact on the material elastic properties. For sizes below ten nanometers, the continuum approach would be outperformed by atomistic simulations [30,31].

4. Conclusions

Our main theoretical result is the equation (11). This equation is exact in terms of big curvature. The equation contains a parameter, the tangential to the electrode surface reaction force component. Hence, fitting of the solutions to experimental data can be used to measure the reaction force acting at the contact. Our results demonstrate that the tangential force component can be comparable or even

bigger than the corresponding normal component. This result is unexpected for the authors and may be important for better understanding of the processes in nano-contacts.

It is clearly beyond the scope of this paper to investigate the origin of the discovered tangential forces. The hypothetical explanation however can be proposed. We believe that when the nanowire's free end hits the electrode surface (when jump to contact takes place) the shape of the nanowire is influenced by the electrostatic attraction forces as well as by the dynamics of the jump. Later, when the electric contact is established and the voltage is switched off, the force distribution along the nanowire changes. The point of contact however in the case of strong adhesion is fixed. As a result, the nanowire may be finally caught by adhesion forces in a slightly stretched/compressed condition. This may change the resonance frequency of the nanowire in contact and affect the following process of the off switching.

Finally, it should be mentioned that we made our best to choose the best nanowire sample. We examined single-clamped nanowire resonant frequencies for different oscillation directions. We inspected our nanowire images to find any sign of variation of diameter along the wire. Despite our efforts, the resonant frequency of the nanowire in contact appeared to be too high relative to its single-clamped frequency. We believe that this is an evidence of non-constant mass and/or elastic property distribution along the length of our sample.

Acknowledgements

This work has been done within the project Nr. 549/2012 of the Latvian Council of Science.

References

1. Loh OY, Espinosa HD (2012) Nanoelectromechanical contact switches. Nat Nanotechnol 7:283–295.
2. Hwang HJ, Kang JW (2005) Carbon-nanotube-based nanoelectromechanical switch. Phys E Low-dimensional Syst Nanostructures 27:163–175.
3. Chen Z, Tong L, Wu Z, Liu Z (2008) Fabrication of electromechanical switch using interconnected single-walled carbon nanotubes. Appl Phys Lett 92:103116.
4. Ke C, Espinosa HD (2006) In situ electron microscopy electromechanical characterization of a

bistable NEMS device. Small 2:1484–1489.

5. Andzane J, Petkov N, Livshits AI, et al (2009) Two-terminal nanoelectromechanical devices based on germanium nanowires. Nano Lett 9:1824–1829.
6. Ziegler KJ, Lyons DM, Holmes JD, et al (2004) Bistable nanoelectromechanical devices. Appl Phys Lett 84:4074–4076.
7. Andzane J, Prikulis J, Dvorsek D, et al (2010) Two-terminal nanoelectromechanical bistable switches based on molybdenum–sulfur–iodine molecular wire bundles. Nanotechnology 21:125706.
8. Lee SW, Lee DS, Morjan RE, et al (2004) A three-terminal carbon nanorelay. Nano Lett 4:2027–2030.
9. Viasnoff V, Meller A, Isambert H (2006) DNA nanomechanical switches under folding kinetics control. Nano Lett 6:101–104.
10. Jang JE, Cha SN, Choi YJ, et al (2008) Nanoscale memory cell based on a nanoelectromechanical switched capacitor. Nat Nanotechnol 3:26–30.
11. Jang WW, Lee JO, Yoon J-B, et al (2008) Fabrication and characterization of a nanoelectromechanical switch with 15-nm-thick suspension air gap. Appl Phys Lett 92:103110.
12. Jang JE, Cha SN, Choi Y, et al (2005) Nanoelectromechanical switches with vertically aligned carbon nanotubes. Appl Phys Lett 87:163114.
13. Rueckes T, Kim K, Joselevich E, et al (2000) Carbon nanotube-based nonvolatile random access memory for molecular computing. Science 289:94–97.
14. Kim P, Lieber CM (1999) Nanotube nanotweezers. Science 286:2148–2150.
15. Kinaret JM, Nord T, Viefers S (2003) A carbon-nanotube-based nanorelay. Appl Phys Lett 82:1287–1289.
16. Andzane J, Meija R, Livshits AI, et al (2013) An AC-assisted single-nanowire electromechanical switch. J Mater Chem C 1:7134–7138. doi: 10.1039/C3TC31240B
17. Holmes JD, Lyons DM, Ziegler KJ (2003) Supercritical fluid synthesis of metal and semiconductor nanomaterials. Chem Eur J 9:2144–2150.
18. Qin Q, Xu F, Cao Y, et al (2012) Measuring True Young's Modulus of a Cantilevered Nanowire: Effect of Clamping on Resonance Frequency. Small 8:2571–2576.

19. Meija R, Kosmaca J, Jasulaneca L, et al (2015) Electric current induced modification of germanium nanowire NEM switch contact. Nanotechnology 26:195503.

20. Meija R, Signetti S, Schuchardt A, et al (2017) Nanomechanics of individual aerographite tetrapods. Nature Communications 8: 14982.

21. Kosmaca J, Jasulaneca L, Meija R, et al (2017) Young's modulus and indirect morphological analysis of Bi2Se3 nanoribbons by resonance measurements. Nanotechnology 28: 325701.

22. Jasulaneca L, Meija R, Livshits AI, et al (2016) Determination of Young's modulus of Sb2S3 nanowires by in situ resonance and bending methods. Beilstein Journal of Nanotechnology 7:278–283.

23. Zhang Y, Zhuo LJ, Zhao HS (2013) Determining the effects of surface elasticity and surface stress by measuring the shifts of resonant frequencies. In: Proc. R. Soc. London A Math. Phys. Eng. Sci. p 20130449

24. Wang Y, Song J, Xiao J (2013) Surface effects on in-plane buckling of nanowires on elastomeric substrates. Journal of Physics D: Applied Physics 46:125309.

25. Timoshenko S (1953) History of strength of materials: With a brief account of the history of theory of elasticity and theory of structures. McGraw-Hill, New York

26. Landau LD, Livshitz EM (2007) Teoriya uprugosti. Fizmatlit, Moscow

27. Wang KF, Wang BL (2015) A general model for nano-cantilever switches with consideration of surface effects and nonlinear curvature. Phys E Low-dimensional Syst Nanostructures 66:197–208.

28. Wolfram Research I (2015) Mathematica, Version 10. Wolfram Research, Inc., Champaign, Illinois

29. Chen CQ, Shi Y, Zhang YS, et al (2006) Size dependence of Young's modulus in ZnO nanowires. Physical Review Letters 96:75505.

30. Miller RE, Shenoy VB (2000) Size-dependent elastic properties of nanosized structural elements. Nanotechnology 11:139.

31. Villain P, Beauchamp P, Badawi KF, et al (2004) Atomistic calculation of size effects on elastic coefficients in nanometre-sized tungsten layers and wires. Scripta Materialia 50:1247–1251.

Appendix

Several nonzero members of the expansion (17).

Expansion members that do not depend on the force model

Indices i,j,k,l	$y_{i,j,k,l}(\xi)$
0,0,1,0	$\frac{1}{4}(-\xi^2+\xi^3)$
0,0,1,1	$\frac{1}{240}(3\xi^2-\xi^3-5\xi^4+3\xi^5)$
0,0,1,2	$\frac{1}{100800}(-66\xi^2+22\xi^3+105\xi^4-21\xi^5-70\xi^6+30\xi^7)$
0,0,1,3	$\frac{1}{100800}(201\xi^2-67\xi^3-330\xi^4+66\xi^5+210\xi^6-30\xi^7+75\xi^8+25\xi^9)$
0,0,3,0	$\frac{1}{13440}(-9\xi^2+17\xi^3+70\xi^4-294\xi^5+378\xi^6-162\xi^7)$
0,0,3,1	$\frac{1}{1612800}(111\xi^2-221\xi^3-1350\xi^4+4218\xi^5-700\xi^6-9348\xi^7+$ $+10935\xi^8-3645\xi^9)$
0,1,0,0	$\frac{1}{2}(3\xi^2-\xi^3)$
0,1,0,1	$\frac{1}{40}(4\xi^2-8\xi^3+5\xi^4-\xi^5)$
0,1,0,2	$\frac{1}{8400}(-24\xi^2+8\xi^3+70\xi^4-84\xi^5+35\xi^6-5\xi^7)$
0,1,0,3	$\frac{1}{3024000}(384\xi^2-128\xi^3-720\xi^4+144\xi^5+840\xi^6-720\xi^7+$ $+225\xi^8-25\xi^9)$
0,1,2,0	$\frac{1}{1120}(-13\xi^2+9\xi^3-105\xi^4+343\xi^5-315\xi^6+81\xi^7)$
0,1,2,1	$\frac{1}{268800}(546\xi^2-558\xi^3+580\xi^4+3636\xi^5+20832\xi^6+31208\xi^7-$ $-18225\xi^8+3645\xi^9)$
0,2,1,0	$\frac{1}{1120}(-51\xi^2+171\xi^3+630\xi^4-1470\xi^5+882\xi^6-162\xi^7)$
0,2,1,1	$\frac{1}{44800}(515\xi^2-513\xi^3+1930\xi^4-13574\xi^5+26628\xi^6-22276\xi^7+$ $+8505\xi^8-1215\xi^9)$
0,3,0,0	$\frac{1}{280}(180\xi^2-144\xi^3-315\xi^4+441\xi^5-189\xi^6+27\xi^7)$
0,3,0,1	$\frac{1}{22400}(1344\xi^2-3072\xi^3-3840\xi^4+18240\xi^5-22344\xi^6+12912\xi^7-$ $-3645\xi^8+405\xi^9)$

Expansion members for the case of constant force density, n=0.

Indices i,j,k,l	$y_{i,j,k,l}(\xi)$
1,0,0,0	$\frac{1}{48}(3\xi^2 - 5\xi^3 + 2\xi^4)$
1,0,0,1	$\frac{1}{2880}(-6\xi^2 + 2\xi^3 + 15\xi^4 - 15\xi^5 + 4\xi^6)$
1,0,0,2	$\frac{1}{403200}(39\xi^2 - 13\xi^3 - 70\xi^4 + 14\xi^5 + 70\xi^6 - 50\xi^7 + 10\xi^8)$
1,0,0,3	$\frac{1}{72576000}(-342\xi^2 + 114\xi^3 + 585\xi^4 - 117\xi^5 - 420\xi^6 + 60\xi^7 + 225\xi^8 - -125\xi^9 + 20\xi^{10})$
1,0,2,0	$\frac{1}{322560}(-159\xi^2 + 53\xi^3 - 1260\xi^4 + 6468\xi^5 - 11060\xi^6 + 8172\xi^7 - 2214\xi^8)$
1,0,2,1	$\frac{1}{6451200}(506\xi^2 - 110\xi^3 + 3095\xi^4 - 13275\xi^5 + 7336\xi^6 + 29536\xi^7 - -53149\xi^8 + 33585\xi^9 - 7524\xi^{10})$
1,1,1,0	$\frac{1}{26880}(-237\xi^2 + 107\xi^3 + 1820\xi^4 - 5628\xi^5 + 7028\xi^6 - 3828\xi^7 + 738\xi^8)$
1,1,1,1	$\frac{1}{1612800}(1530\xi^2 - 310\xi^3 - 4125\xi^4 - 14043\xi^5 + 8285\xi^6 - 147012\xi^7 + +122529\xi^8 - 48945\xi^9 + 7524\xi^{10})$
1,2,0,0	$\frac{1}{8960}(-683\xi^2 + 1329\xi^3 - 2380\xi^4 + 4340\xi^5 - 4004\xi^6 + 1644\xi^7 - 246\xi^8)$
1,2,0,1	$\frac{1}{537600}(1794\xi^2 - 222\xi^3 - 15455\xi^4 + 62283\xi^5 - 123200\xi^6 + 129496\xi^7 - -72623\xi^8 + 21435\xi^9 - 2508\xi^{10})$
2,0,1,0	$\frac{1}{967680}(159\xi^2 - 98\xi^3 + 945\xi^4 - 5733\xi^5 + 1224\xi^6 - 12699\xi^7 + +6483\xi^8 - 1300\xi^9)$
2,0,1,1	$\frac{1}{2554675200}(-63873\xi^2 + 30619\xi^3 - 256080\xi^4 + 1325940\xi^5 - 1130052\xi^6 - -2998908\xi^7 + 7583103\xi^8 - 7004965\xi^9 + 3022536\xi^{10} - 508320\xi^{11})$
2,1,0,0	$\frac{1}{967680}(1761\xi^2 - 875\xi^3 - 10710\xi^4 + 34146\xi^5 - 52122\xi^6 + 41958\xi^7 - -16785\xi^8 + 2600\xi^9)$
2,1,0,1	$\frac{1}{425779200}(-79216\xi^2 + 30688\xi^3 + 138490\xi^4 + 664510\xi^5 - 368670\xi^6 + 7376160\xi^7 - -7747311\xi^8 + 4501255\xi^9 - 1367256\xi^{10} + 169440\xi^{11})$
3,0,0,0	$\frac{1}{46448640}(-603\xi^2 + 417\xi^3 - 3780\xi^4 + 26460\xi^5 - 67788\xi^6 + 90180\xi^7 - -66726\xi^8 + 26000\xi^9 - 4160\xi^{10})$

3,0,0,1	$\frac{1}{30656102400}(57498\xi^2 - 31574\xi^3 + 216315\xi^4 - 1266903\xi^5 + 1319472\xi^6 + +3262248\xi^7 - 10434303\xi^8 + 12500675\xi^9 - 7826148\xi^{10} + 2541600\xi^{11} - 338880\xi^{12}\}$

Expansion members for the case of parabolic force density, n=1.

Indices i,j,k,l	$y_{i,j,k,l}(\xi)$
1,0,0,0	$\frac{1}{120}(9\xi^2 - 13\xi^3 + 6\xi^5 - 2\xi^6)$
1,0,0,1	$\frac{1}{33600}(-87\xi^2 + 29\xi^3 + 210\xi^4 - 182\xi^5 + 40\xi^7 - 10\xi^8)$
1,0,0,2	$\frac{1}{6048000}(726\xi^2 - 242\xi^3 - 1305\xi^4 + 261\xi^5 + 1260\xi^6 - 780\xi^7 + +100\xi^9 - 20\xi^{10})$
1,0,0,3	$\frac{1}{13970880000}(-81561\xi^2 + 27187\xi^3 + 139755\xi^4 - 27951\xi^5 - 100485\xi^6 + +14355\xi^7 + 51975\xi^8 - 25025\xi^9 + 2100\xi^{11} - 350\xi^{12})$
1,0,2,0	$\frac{1}{268800}(-81\xi^2 + 33\xi^3 - 1400\xi^4 + 6160\xi^5 - 8820\xi^6 + 2932\xi^7 + 3950\xi^8 - -3620\xi^9 + 846\xi^{10})$
1,0,2,1	$\frac{1}{3725568000}(191133\xi^2 - 28599\xi^3 + 2431275\xi^4 - 8804565\xi^5 + 2377914\xi^6 + +24052314\xi^7 - 33322905\xi^8 + 7946015\xi^9 + 12560548\xi^{10} - 9269820\xi^{11} + 1866690\xi^{12})$
1,1,1,0	$\frac{1}{33600}(-198\xi^2 - 47\xi^3 + 2730\xi^4 - 7812\xi^5 + 7686\xi^6 - 186\xi^7 - -4170\xi^8 + 2420\xi^9 - 423\xi^{10})$
1,1,1,1	$\frac{1}{310464000}(196080\xi^2 + 43056\xi^3 - 764610\xi^4 - 3288516\xi^5 + 17660874\xi^6 - -27078018\xi^7 + 12964875\xi^8 + +7246855\xi^9 - 10735186\xi^{10} + 4376820\xi^{11} - 622230\xi^{12})$
1,2,0,0	$\frac{1}{22400}(-1725\xi^2 + 3337\xi^3 - 6720\xi^4 + 11760\xi^5 - 7308\xi^6 - 2436\xi^7 + +4830\xi^8 - 2020\xi^9 + 282\xi^{10})$
1,2,0,1	$\frac{1}{103488000}(287097\xi^2 + 50909\xi^3 - 3322935\xi^4 + 13334013\xi^5 - 23867382\xi^6 + +17999586\xi^7 + 241395\xi^8 - 9606905\xi^9 + 6564712\xi^{10} - 1887900\xi^{11} + 207410\xi^{12})$
2,0,1,0	$\frac{1}{576576000}(82713\xi^2 - 68703\xi^3 + 930930\xi^4 - 4510506\xi^5 + 7261254\xi^6 - -2250534\xi^7 - 6091800\xi^8 + 6380660\xi^9 - 586014\xi^{10} - 2102100\xi^{11} + 1139320\xi^{12} - 185220\xi^{13})$

2,0,1,1	$\frac{1}{484323840000}(-11115675\xi^2 + 6478559\xi^3 - 83699490\xi^4 + 337930950\xi^5$ $- 121705584\xi^6 - 1098861192\xi^7 + 1766739975\xi^8 -$ $-389108005\xi^9 - 1212340558\xi^{10} + 1026785760\xi^{11} -$ $-63843780\xi^{12} - 263069520\xi^{13} + 123680400\xi^{14} - 17871840\xi^{15})$
2,1,0,0	$\frac{1}{96096000}(191505\xi^2 - 53461\xi^3 - 1471470\xi^4 + 4210206\xi^5 - 4450446\xi^6 -$ $-462462\xi^7 + 4611750\xi^8 -$ $-2882880\xi^9 - 462462\xi^{10} + 1173900\xi^{11} - 465920\xi^{12} + 61740\xi^{13})$
2,1,0,1	$\frac{1}{80720640000}(-15900057\xi^2 + 3969801\xi^3 + 32023950\xi^4 + 168541254\xi^5 -$ $-462462\xi^7 + 4611750\xi^8 - 831670125\xi^9 + 1031573686\xi^{10} -$ $-275129400\xi^{11} - 216301540\xi^{12} + 187211640\xi^{13} - 55038000\xi^{14} + 5957280\xi^{15})$
3,0,0,0	$\frac{1}{11531520000}(-185145\xi^2 + 156633\xi^3 + 1801800\xi^4 + 9993984\xi^5 -$ $-18270252\xi^6 + 6333756\xi^7 + 21282690\xi^8 - 26137540\xi^9 + 894894\xi^{10} +$ $+16325400\xi^{11} - 9529520\xi^{12} - 1040760\xi^{13} + 2934000\xi^{14} - 1092960\xi^{15} + 136620\xi^{16})$
3,0,0,1	$\frac{1}{82335052800000}(191571816\xi^2 - 124610818\xi^3 + 1208486055\xi^4 - 5427674133\xi^5 +$ $+2251042794\xi^6 + 21120717618\xi^7 - 38227608705\xi^8 + 8984040065\xi^9 +$ $+36296478218\xi^{10} - 35275312800\xi^{11} - 32316830\xi^{12} + 16830129540\xi^{13} -$ $-8641542000\xi^{14} - 312789120\xi^{15} + 1654159500\xi^{16} - 556617600\xi^{17} + 61846400\xi^{18})$

- Finite kurvature bent beam (nanowire) equation of motion is proposed.
- The solution is used to investigate the experimental nano-switch contact.
- A strong tangential component of the reaction at nano-switch contact is found.